Received: 9 September 2016 | Revised: 11 July 2017 | Accepted: 26 September 2017

DOI: 10.1002/nag.2754

RESEARCH ARTICLE

WILEY

Bearing capacity of foundations on rock mass using the method of characteristics

Amin Keshavarz[1] | Jyant Kumar[2]

[1] School of Engineering, Persian Gulf University, Bushehr, Iran

[2] Civil Engineering Department, Indian Institute of Science, Bangalore, India

Correspondence
Jyant Kumar, Civil Engineering Department, Indian Institute of Science, Bangalore 560012, India.
Email: jkumar@iisc.ac.in

Summary

The method of stress characteristics has been used for computing the ultimate bearing capacity of strip and circular footings placed on rock mass. The modified Hoek-and-Brown failure criterion has been used. Both smooth and rough footing-rock interfaces have been modeled. The bearing capacity has been expressed in terms of nondimensional factors $N_{\sigma 0}$ and N_{σ}, corresponding to rock mass with (1) $\gamma = 0$ and (2) $\gamma \neq 0$, respectively. The numerical results have been presented as a function of different input parameters needed to define the Hoek-and-Brown criterion. Slip line patterns and the pressure distribution along the footing base have also been examined. The results are found to compare generally well with the reported solutions.

KEYWORDS

bearing capacity, failure, foundations, Hoek-Brown criterion, rocks, the method of characteristics

1 | INTRODUCTION

The determination of the bearing capacity of footings on rocks forms an important issue especially while (1) laying foundations on weak rocks, (2) estimating the ultimate tip resistance of piles placed on rocks, and (3) designing dams' foundations. As compared with foundations in soils, only limited studies seem to have been available in literature to compute the bearing capacity of foundations on rock mass. Serrano and Olalla used the Hoek-and-Brown (HB) failure criterion to compute the ultimate bearing capacity of strip footings placed on a weightless rock medium.[1] Serrano et al also used the modified HB criterion to evaluate the bearing capacity of a strip footing placed on a weightless rock medium.[2] By using the original HB criterion, Yang et al performed a lower-bound limit analysis to compute the bearing capacity of a strip footing placed on a weightless rock medium.[3] Merifield et al used the limit analysis in combination with optimization and finite elements to compute the ultimate bearing capacity of strip footings on rock mass.[4] In this analysis, the modified HB failure criterion was used to compute the ultimate bearing capacity. By using the original and modified HB failure criteria, Zhou et al applied the slip line method to calculate the bearing capacity of strip footings placed on rock mass.[5] Clausen used the standard displacement-based elastoplastic finite element approach to compute the ultimate bearing capacity of circular footings laid on rock mass.[6] Chakraborty and Kumar evaluated the ultimate bearing capacity of circular footings on rock mass by using the lower-bound theorem of the limit analysis.[7] In this work, the modified HB failure criterion was used but by assuming a constant value of the exponent, $a = 0.5$, which provides an overestimation of the bearing capacity for lower values of the geological strength index (*GSI*). Keshavarz et al used the method of stress characteristics to evaluate the seismic bearing capacity of strip footings placed over rock mass.[8] The study was, however, based on the original HB failure criterion, and moreover, it did not consider a formation of a nonplastic wedge, which invariably occurs for a rough footing base. As compared with available solutions for strip footings, not many theories seem to be existing for finding the bearing capacity of

circular footings placed on rock mass. The studies of Clausen[6] and Chakraborty and Kumar[7] seem to be perhaps the only ones for the circular foundations.

The objective of the present study is to evaluate the ultimate bearing capacity of strip and circular footings placed on rock mass by using the method of stress characteristics. The modified HB failure criterion has been used. The analysis has been performed for both smooth and rough footing-rock interfaces. The effects of different material input parameters needed to define the modified HB failure criterion completely on the resulting bearing capacity, pressure distribution, and failure patterns have been examined. The results obtained from the analysis have been compared with that available from the literature.

2 | MODIFIED HB FAILURE CRITERION

The modified HB failure criterion[9] can be written as

$$\frac{\sigma_1-\sigma_3}{\sigma_c}=\left(m_b\frac{\sigma_3}{\sigma_c}+s\right)^a, \tag{1}$$

where (1) σ_c defines the uniaxial compressive strength of the intact rock mass; (2) σ_1 and σ_3 represent the major and minor principal stresses, respectively; and (3) a, m_b, and s represent the dimensionless input material parameters, which are defined as follows[10]:

$$\begin{aligned} a&=\frac{1}{2}+\frac{1}{6}\left\{\exp\left(\frac{-GSI}{15}\right)-\exp\left(\frac{-20}{3}\right)\right\},\\ m_b&=m_i\exp\left(\frac{GSI-100}{28-14D}\right),\\ s&=\exp\left(\frac{GSI-100}{9-3D}\right). \end{aligned} \tag{2}$$

In the above expressions, *GSI* refers to the geological strength index and the factor D represents the disturbance of the rock mass, the value of which varies from 0 for an undisturbed rock mass to 1 for very disturbed rock mass. Unless otherwise exclusively specified, the value of D has been assumed to be 0 in the present analysis.

3 | EQUILIBRIUM EQUATIONS

All the basic equations have been presented only for an axisymmetric case. However, these equations can be easily transformed to an equivalent plane strain case by simply replacing the basic stress variables σ_r, σ_z, and τ_{rz} with σ_x, σ_y, and τ_{xy}, respectively. The axisymmetric problem also involves an additional circumferential stress variable σ_θ; on the basis of the Harr-Von Karman hypothesis, the value of σ_θ has been assumed to be equal to the minor principal stress σ_3. With reference to Figure 1A, for an axisymmetric case in an r-z plane, the equilibrium equations are given as

$$\begin{aligned} \frac{\partial\sigma_r}{\partial r}+\frac{\partial\tau_{rz}}{\partial z}&=f_r,\\ \frac{\partial\sigma_z}{\partial z}+\frac{\partial\tau_{rz}}{\partial r}&=f_z. \end{aligned} \tag{3}$$

Here, the parameters f_r and f_z are defined by the following expressions:

$$\begin{aligned} f_r&=-\frac{n}{r}(\sigma_r-\sigma_\theta),\\ f_z&=-\gamma-\frac{n}{r}\tau_{rz}. \end{aligned} \tag{4}$$

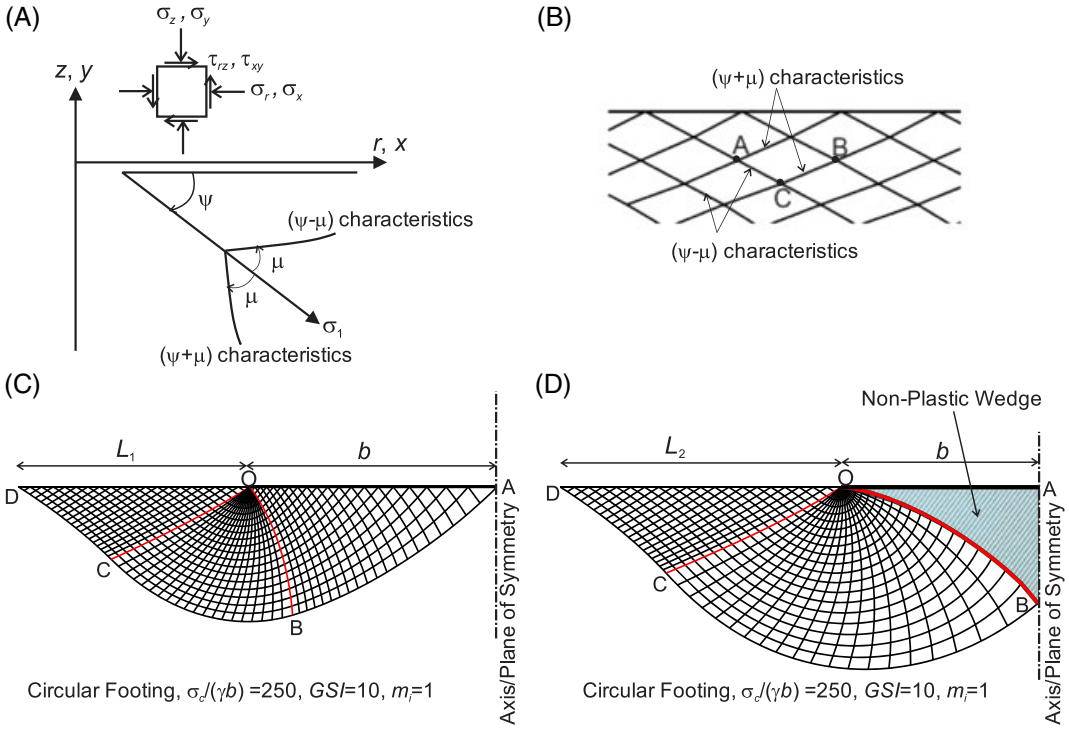

FIGURE 1 A, Definition of stress variables and stress characteristics. B, Finding unknown variables at the point C from the known variables at points A and B. C, Characteristic patterns for a smooth footing. D, Characteristic patterns for a rough footing [Colour figure can be viewed at wileyonlinelibrary.com]

The value of n in Equation 4 becomes equal to 0 and 1, corresponding to plane strain and axisymmetric cases, respectively, and γ forms the unit weight of the rock mass.

The generalized failure criterion for a homogenous medium can be written in the following form[11]:

$$f(\sigma_z, \sigma_r, \tau_{rz}) = R - F(p, \psi) = 0, \tag{5}$$

where $p = \sigma_r + \sigma_z/2$, R is the radius of the Mohr circle, and the parameter ψ represents the angle between the positive r axis and the direction of the major principal stress (σ_1). On the basis of the Mohr circle, the 3 basic stress variables (σ_r, σ_z, and τ_{rz}) are written in terms of 2 stress variables as

$$\begin{aligned} \sigma_r &= p + R\ \cos 2\psi, \\ \sigma_z &= p - R\ \cos 2\psi, \\ \tau_{rz} &= \mathrm{R}\ \sin 2\psi. \end{aligned} \tag{6}$$

With Equations 3 and 6, the associated expressions that are applicable along 2 different families of characteristics are established[12]:

- Along the $(\psi + \mu)$ characteristics:

$$\mathrm{d}z/\mathrm{d}r = \tan(\psi - m + \mu) \tag{7}$$

$$\frac{\sin 2(m+\mu)}{\cos 2m}\mathrm{d}p + \frac{2R}{\cos 2m}\mathrm{d}\psi = (\mathrm{d}r \sin 2\mu - \mathrm{d}z \cos 2\mu) f_r + (\mathrm{d}r \cos 2\mu + \mathrm{d}z \sin 2\mu) f_z \tag{8}$$

- Along the $(\psi - \mu)$ characteristics:

$$\mathrm{d}z/\mathrm{d}r = \tan(\psi - m - \mu) \tag{9}$$

$$\frac{\sin 2(m-\mu)}{\cos 2m}\mathrm{d}p + \frac{2R}{\cos 2m}\mathrm{d}\psi = -(\mathrm{d}r\sin 2\mu + \mathrm{d}z\cos 2\mu)f_r + (\mathrm{d}r\cos 2\mu - \mathrm{d}z\sin 2\mu)f_z \tag{10}$$

where

$$\begin{aligned} \tan 2m &= \frac{1}{2R}\frac{\partial R}{\partial \psi} \\ \cos 2\mu &= \cos 2m\,\frac{\partial R}{\partial p} \end{aligned} \tag{11}$$

After algebraic simplifications, Equation 11 can be rewritten as

$$\frac{R}{\beta_a}\left(1 + (1-a)\left(\frac{R}{\beta_a}\right)^k\right) = \frac{p}{\beta_a} + \zeta_a. \tag{12}$$

Here,

$$\zeta_a = \frac{s}{m_b A_a}; \quad \beta_a = A_a\sigma_c; \quad k = \frac{1-a}{a}; {A_a}^k = \frac{m_b(1-a)}{\frac{1}{2a}} \tag{13}$$

By using Equations 11 and 12, the values of m and μ can be computed as

$$m = 0; \qquad \mu = 0.5\cos^{-1}\left(\frac{1}{1 + (1-a)\left(\frac{R}{\beta_a}\right)^k(1+k)}\right). \tag{14}$$

From the rock mass properties and the value of p, one can calculate R on the basis of Equation 12 by using the Newton-Raphson method. In the method of stress characteristics, each point has 4 basic variables, namely, r, z, p, and ψ: (1) the first 2 variables r and z provide the location of the point and (2) the remaining 2 variables, which are p and ψ, provide the corresponding state of stress at failure. With reference to Figure 1B, the 4 unknown variables for point C in the stress characteristics network can be found from the known values of the associated parameters from the previous points A and B, where AC and BC refer to the $(\psi - \mu)$ and $(\psi + \mu)$ characteristics, respectively.

A trial-and-error procedure needs to be used to establish point C and its corresponding state of stress from Equations 7 to 10. In the first iteration, the stress variables for point C are first assumed to be equal to the mean of the corresponding values at points B and A. The new values are then established at point C. These obtained values are then used again to update the results. This procedure is continued until the difference between the variables' values between the current and previous iterations becomes less than 0.0001%.

4 | SOLUTION PROCEDURE

4.1 | Smooth footing

Figure 1C shows the stress characteristics patterns for a smooth footing. In this Figure, OA defines the footing base, and the parameter b refers to (1) the footing radius for a circular footing and (2) half the footing width for a strip footing. A uniform surcharge pressure q is prescribed along the boundary OD. Along this boundary, the normal stress σ_0 becomes equal to q and the shear stress τ_0 is 0. Accordingly, the value of ψ along this boundary (ψ_0) becomes equal to 0. By using the Mohr stress circle, one can write

$$R_0 = \sqrt{(p_0 - \sigma_0)^2 + \tau_0}. \tag{15}$$

Therefore, $R_0 = p_0 - q$ and Equation 12 along the boundary OD can be written as

$$\frac{p_0 - q}{\beta_a}\left\{1 + (1-a)\left(\frac{p_0 - q}{\beta_a}\right)^k\right\} = \frac{p_0}{\beta_a} + \zeta_a. \tag{16}$$

The value of the mean stress along this boundary p_0 can be obtained by solving Equation 16. This equation is then solved by using the Newton-Raphson iterative technique.

Along the footing-rock interface boundary (boundary OA in Figure 1C), the normal stress q_f is unknown. Along the smooth footing base, the direction of σ_1 becomes vertical; therefore,

$$\begin{aligned} &\psi_f = \pi/2, \\ &\sigma_z = q_f = p_f + R_f. \end{aligned} \tag{17}$$

As shown in Figure 1C, the stress characteristic network includes 3 zones: OAB, OCD, and OBC zones. The solution starts from the known state of stress along the boundary OD. This boundary is divided into n_1 number of points, and the coordinates r and z of each point are calculated. The values of ψ_0 for all these points are 0, and the values of p_0 are then calculated from Equation 16. From the known state of stress along the line OD, the state of stress and the characteristic pattern in the zones OBC and OCD are then calculated by using the finite difference technique.

Note that at point O, there remains a stress singularity since the state of stress remains different on its left and right sides. At this point, $dr = dz = 0$, and Equation 10 changes to

$$-\sin 2\mu dp + 2R d\psi = 0. \tag{18}$$

To deal with this stress singularity, a very small zone around the converging stress characteristics at this point is divided into n_g number of divisions. To find the value of p at each point, the finite difference form of Equation 18 is used.

By integrating the vertical normal stress along the footing base OA, the ultimate bearing capacity q_u is computed as follows:

- Strip footing:

$$q_u = \frac{1}{b}\int_{OA} \sigma_z dr \tag{19a}$$

- Circular footing:

$$q_u = \frac{2}{b^2}\int_{OA} \sigma_z r dr \tag{19b}$$

4.2 | Rough footing

For a rough footing, the major principal stress at $r = z = 0$ must be vertical along the footing base ($\psi = \pi/2$). If the full roughness is mobilized at any point, then the converging characteristics need to be tangential to the footing base,[13,14] $\psi_f = \pi - \mu_f$.

$$\psi_f = \pi - 0.5\cos^{-1}\left(\frac{1}{\left\{1+(1-a)\left(\frac{R_f}{\beta_a}\right)^k(1+k)\right\}}\right) \tag{20}$$

Figure 1D illustrates the stress characteristic patterns for a rough footing. Along the stress characteristic OB, which becomes the boundary of the nonplastic zone below the footing, the direction of the major principal stress becomes vertical. The solution procedure becomes similar to that for a smooth footing, but the slip line patterns involve only 2 zones, namely, OCD and OBC; the region OBC is often termed as the radial shear zone. For a chosen value of b, the values of ψ at the right side of point O and L_2 should be obtained such that at point B, $r = 0$ and $\psi = \pi/2$. A trial and iterative procedure is used for doing the necessary computations to establish the state of stress everywhere along the characteristic OB.

TABLE 1 The variation of N_σ with the number of divisions for different combinations of GSI, m_i, and $\sigma_c/(\gamma b)$ ($n_g = n_1$) for $q/\sigma_c = 0$ and $D = 0$

Cases	Footing, Base	$n_1 = 10$	$n_1 = 20$	$n_1 = 40$	$n_1 = 80$	$n_1 = 100$	$n_1 = 150$	$n_1 = 200$	$n_1 = 250$	$n_1 = 300$
Case 1:	Circular, rough	0.03714	0.03802	0.03845	0.03866	0.03871	0.03876	0.03879	0.03880	0.03880
$GSI = 15$,	Circular, smooth	0.03271	0.03357	0.03397	0.03416	0.03419	0.03419	0.03419	0.03419	0.03419
$m_i = 1$,	Strip, rough	0.02443	0.02571	0.02636	0.02669	0.02676	0.02685	0.02690	0.02692	0.02692
$\sigma_c/(\gamma b) = \propto$	Strip, smooth	0.02444	0.02571	0.02636	0.02669	0.02676	0.02685	0.02690	0.02690	0.02690
Case 2:	Circular, rough	0.05207	0.05291	0.05328	0.05346	0.05349	0.05354	0.05354	0.05354	0.05354
$GSI = 15$,	Circular, smooth	0.04230	0.04316	0.04353	0.04369	0.04372	0.04376	0.04378	0.04378	0.04378
$m_i = 1$,	Strip, rough	0.04356	0.04567	0.04671	0.04723	0.04733	0.04744	0.04750	0.04754	0.04754
$\sigma_c/(\gamma b) = 125$	Strip, smooth	0.03645	0.03842	0.03940	0.03990	0.04000	0.04013	0.04019	0.04023	0.04023
Case 3:	Circular, rough	0.9765	0.9535	0.9508	0.9518	0.9522	0.9524	0.9526	0.9528	0.9528
$GSI = 25$,	Circular, smooth	0.8159	0.8081	0.8092	0.8107	0.8111	0.8115	0.8119	0.8121	0.8121
$m_i = 20$,	Strip, rough	0.4990	0.5140	0.5243	0.5302	0.5314	0.5331	0.5340	0.5346	0.5346
$\sigma_c/(\gamma b) = \propto$	Strip, smooth	0.5010	0.5142	0.5243	0.5302	0.5314	0.5331	0.5340	0.5346	0.5346
Case 4:	Circular, rough	1.324	1.324	1.326	1.328	1.328	1.328	1.328	1.328	1.328
$GSI = 25$,	Circular, smooth	1.059	1.068	1.072	1.074	1.074	1.074	1.075	1.075	1.075
$m_i = 20$,	Strip, rough	0.9080	0.9490	0.9701	0.9806	0.9826	0.9847	0.9858	0.9864	0.9864
$\sigma_c/(\gamma b) = 125$	Strip, smooth	0.7986	0.8363	0.8560	0.8659	0.8679	0.8706	0.8719	0.8727	0.8727

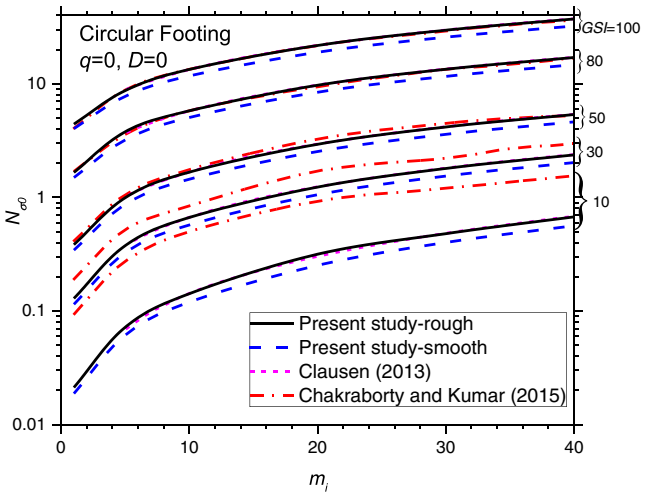

FIGURE 2 The variation of $N_{\sigma 0}$ with m_i and GSI for smooth and rough circular footing and comparison with the existing results for a rough base [Colour figure can be viewed at wileyonlinelibrary.com]

The ultimate bearing capacity q_u for the rough footing is calculated by using the approach similar to that of Kumar[13] by integrating the stress components along the OB:

- For a strip footing:

$$q_u = \frac{1}{b}\int_{OB}\{\sigma_z dr + \gamma z dr + \tau_{rz} dz\} \tag{21a}$$

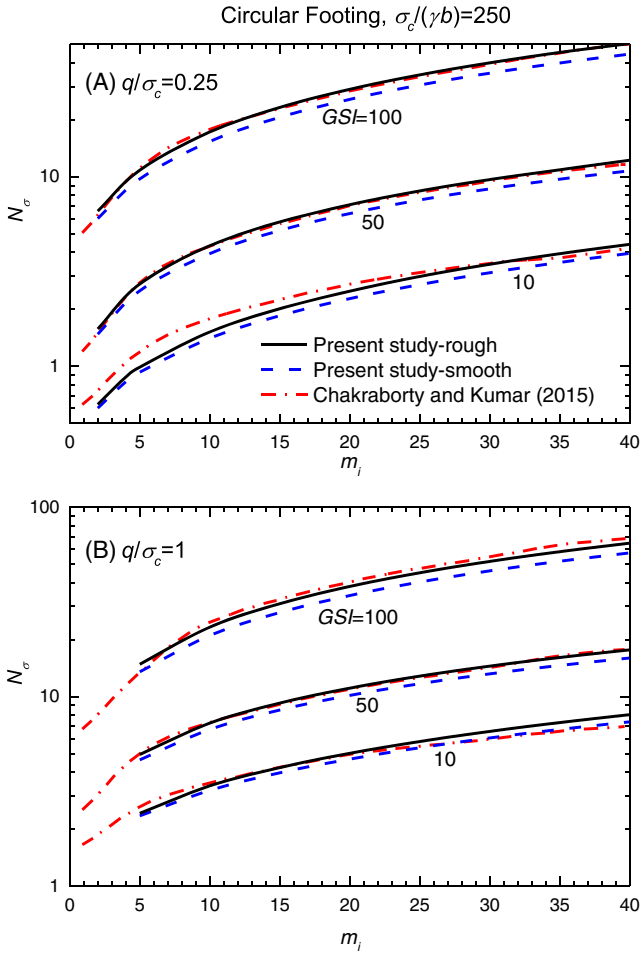

FIGURE 3 The variation of N_σ with m_i and *GSI* for smooth and rough circular footing and comparison with the existing results for a rough base. A, $q/\sigma_c = 0.25$. B, $q/\sigma_c = 1$ [Colour figure can be viewed at wileyonlinelibrary.com]

TABLE 2 The variation of N_σ with *GSI*, $\sigma_c/(\gamma b)$, and m_i for a circular footing with smooth and rough base and its comparison with the results of Clausen[6] for a rough base

GSI	$\sigma_c/(2\gamma b)$	m_i	N_σ, Clausen[6]	N_σ, This Study, Smooth	N_σ, This Study, Rough
10	125	7.5	0.176	0.137	0.174
20	2000	22.5	0.851	0.707	0.846
30	∞	22.5	1.381	1.176	1.351
40	250	35	3.544	2.963	3.519
50	5000	10	1.678	1.446	1.661
60	∞	35	7.053	6.053	6.940
80	500	10	5.818	5.049	5.788
100	250	22.5	23.91	20.664	23.787

TABLE 3 The variation of $N_{\sigma 0}$ with *GSI*, $\sigma_c/(\gamma b)$, and m_i for a strip footing with smooth and rough bases and comparison with the results of Merifield et al[4] and Chakraborty and Kumar[7] with a rough base

GSI	m_i	This Study, Smooth	This Study, Rough	Chakraborty and Kumar[7]	Merifield et al[4]
10	1	0.015	0.015	0.014	0.015
	5	0.042	0.042	0.04	0.042
	10	0.076	0.077	0.075	0.077
	20	0.153	0.153	0.151	0.156
	30	0.236	0.237	0.23	0.238
	35	0.281	0.281	0.276	0.288
20	1	0.043	0.043	0.042	0.044
	5	0.117	0.117	0.117	0.119
	10	0.206	0.206	0.204	0.209
	20	0.384	0.384	0.377	0.389
	30	0.567	0.567	0.567	0.575
	35	0.660	0.660	0.662	0.67
30	1	0.091	0.090	0.09	0.092
	5	0.235	0.232	0.23	0.235
	10	0.397	0.393	0.388	0.397
	20	0.710	0.702	0.701	0.713
	30	1.020	1.007	1.015	1.022
	35	1.174	1.159	1.182	1.193
40	1	0.163	0.163	0.161	0.165
	5	0.396	0.396	0.399	0.401
	10	0.652	0.652	0.647	0.659
	20	1.132	1.132	1.138	1.149
	30	1.596	1.597	1.616	1.63
	35	1.825	1.826	1.846	1.873
50	1	0.280	0.277	0.272	0.281
	5	0.644	0.637	0.631	0.644
	10	1.036	1.025	1.028	1.037
	20	1.762	1.742	1.739	1.765
	30	2.456	2.426	2.406	2.467
	35	2.796	2.762	2.766	2.817
60	1	0.460	0.460	0.461	0.465
	5	1.001	1.002	1.009	1.013
	10	1.578	1.578	1.567	1.597
	20	2.632	2.633	2.6	2.667
	30	3.631	3.632	3.592	3.644
	35	4.119	4.120	4.049	4.186
70	1	0.764	0.756	0.761	0.765
	5	1.580	1.564	1.571	1.582
	10	2.441	2.415	2.415	2.444
	20	4.006	3.961	3.978	4.012
	30	5.480	5.417	5.437	5.491
	35	6.198	6.125	6.036	6.068
80	1	1.245	1.245	1.251	1.26
	5	2.444	2.444	2.456	2.473
	10	3.700	3.700	3.712	3.745
	20	5.965	5.966	5.983	6.04
	30	8.086	8.088	8.085	8.195
	35	9.116	9.118	9.118	9.242
90	1	2.078	2.057	2.065	2.083
	5	3.875	3.835	3.846	3.881
	10	5.750	5.689	5.724	5.758

(Continues)

TABLE 3 (Continued)

GSI	m_i	This Study, Smooth	This Study, Rough	Chakraborty and Kumar[7]	Merifield et al[4]
	20	9.114	9.015	9.086	9.125
	30	12.251	12.114	12.198	12.27
	35	13.771	13.616	13.618	13.794
100	1	3.416	3.416	3.433	3.461
	5	6.049	6.050	6.095	6.124
	10	8.790	8.791	8.798	8.896
	20	13.678	13.681	13.789	13.847
	30	18.213	18.217	18.398	18.444
	35	20.404	20.409	20.587	20.668

- For a circular footing:

$$q_u = \frac{1}{\pi b^2} \int_{OB} \{\sigma_z (2\pi r) dr + \gamma z (2\pi r) dr + \tau_{rz} (2\pi r) dz\} \tag{21b}$$

5 | DEFINITION OF BEARING CAPACITY FACTORS

The ultimate bearing capacity (q_u) is expressed in terms of a nondimensional bearing capacity factor N_σ as given herein:

$$q_u = \sigma_c N_\sigma, \tag{22}$$

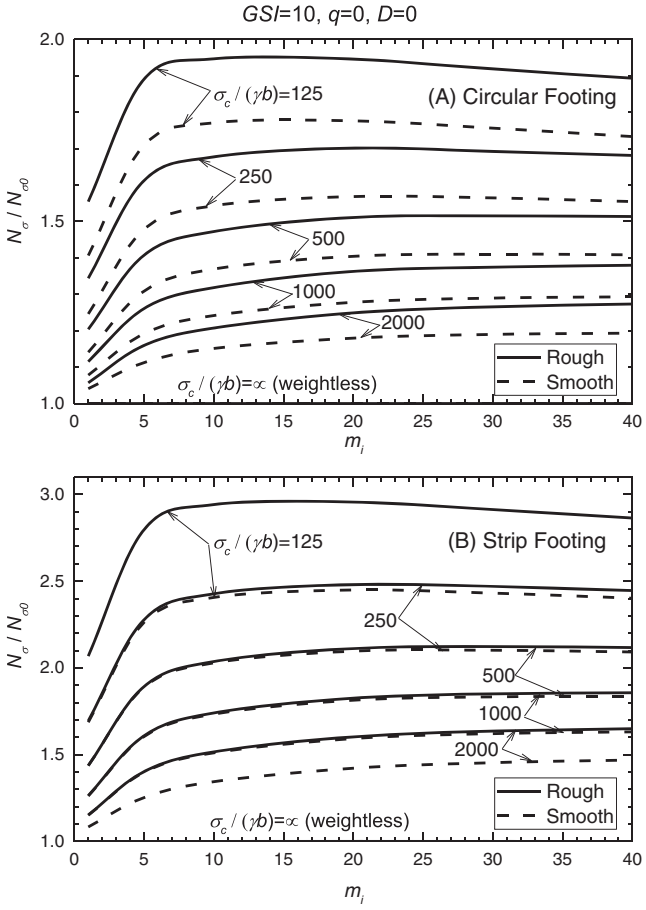

FIGURE 4 The variation of $N_\sigma/N_{\sigma 0}$ with m_i and $\sigma_c/(\gamma b)$ for $GSI = 10$, $q = 0$, and $D = 0$ with smooth and rough bases for (A) circular footing and (B) strip footing

where N_σ is a nondimensional bearing capacity factor, which is simply termed as $N_{\sigma 0}$ for a weightless rock mass ($\gamma = 0$).

6 | RESULTS

6.1 | Convergence check

It is understood from the work of Martin[15] that the accuracy of the obtained solution can be increased by using a large number of characteristics along the ground surface and at the footing edge (singular point). This can be done by increasing the values of the input parameters n_1 and n_g as defined earlier; note that n_1 provides the number of divisions along the ground surface and n_g refers to the number of divisions kept to model the singular point. The values of n_1 and n_g were increased till the value of the bearing capacity factor becomes more or less constant up to the fourth significant digit. To illustrate the convergence of the obtained solution, the values of the bearing capacity factor were determined for the following 4 cases by keeping $q/\sigma_c = 0$ and $D = 0$: (1) case 1, $GSI = 15$, $m_i = 1$, and $\sigma_c/(\gamma b) = \propto$; (2) case 2, $GSI = 15$, $m_i = 1$, and $\sigma_c/(\gamma b) = 125$; (3) case 3, $GSI = 25$, $m_i = 20$, and $\sigma_c/(\gamma b) = \propto$; and (4) case 4: $GSI = 25$, $m_i = 20$, and $\sigma_c/(\gamma b) = 125$. The results corresponding to these 4 cases are presented in Table 1 for both smooth and rough footing bases; the results in all the cases were provided in terms of 4 significant digits. The value of n_g was kept equal to that of n_1. Calculations were conducted by increasing the value of n_1 from 10 to 300. It can be observed that for most cases, the optimum value of n_1 becomes equal to 250. Note that for a weightless rock mass, $\sigma_c/(\gamma b) = \propto$, the bearing capacity of smooth and rough strip footings becomes almost the same. However, when the weight of the rock mass is considered, the bearing capacity of a rough footing becomes greater than that for a smooth footing.

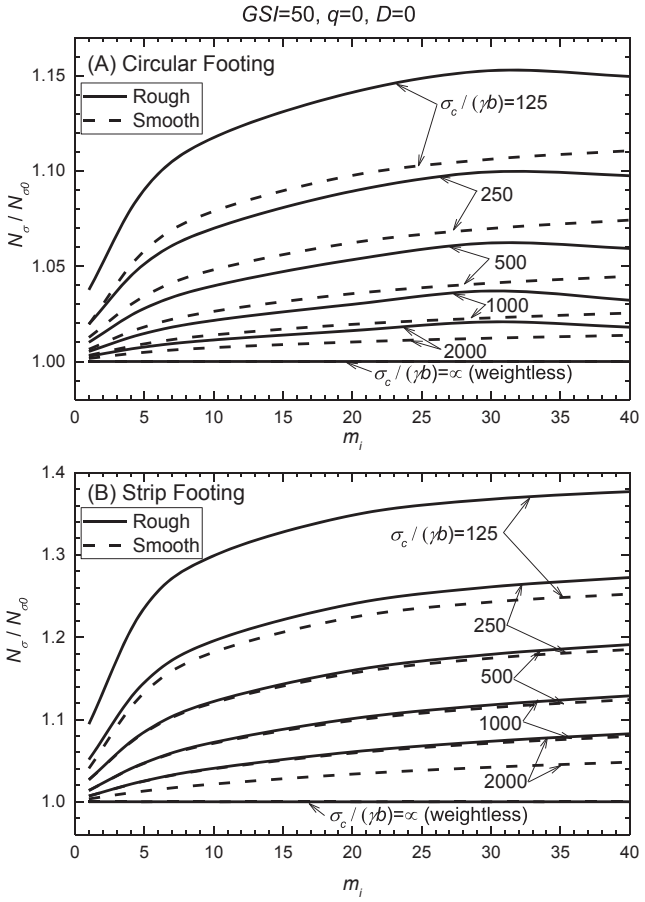

FIGURE 5 The variation of $N_\sigma/N_{\sigma 0}$ with m_i and $\sigma_c/(\gamma b)$ for $GSI = 50$, $q = 0$, and $D = 0$ with smooth and rough bases for (A) circular footing and (B) strip footing

6.2 | Variation of the bearing capacity factors

Figure 2 presents the values of $N_{\sigma 0}$ obtained from the present study for both smooth and rough circular footings. The values of $N_{\sigma 0}$ for a smooth footing for all the values of *GSI* become smaller than those for a rough footing. The maximum difference between the values of $N_{\sigma 0}$ for smooth and rough footings is found to be around 25%. The factor $N_{\sigma 0}$ increases continuously with an increase in the values of m_i and *GSI*. In this figure, a comparison of the results from the present analysis has also been made with that reported by (1) Clausen[6] on the basis of an elastoplastic finite element method for a rough footing and (2) Chakraborty and Kumar[7] by using the lower-bound finite element limit analysis for a rough footing but with an assumption $a = 0.5$. Note that the present results are found to be almost the same as that reported by Clausen.[6] The analysis of Chakraborty and Kumar[7] overestimates the values of $N_{\sigma 0}$, especially for values of $GSI < 50$. It can be noted from Equation 2 that when the value of *GSI* increases from 10 to 100, the magnitude of the exponent a reduces from 0.58 to 0.5. Therefore, as the *GSI* reduces, especially below 50, the difference between the present results and that given by Chakraborty and Kumar[7] is found to become quite extensive. Similar observations with reference to the effect of exponent a on the results have been indicated by Clausen[16] while discussing the results of Chakraborty and Kumar.[7]

Figure 3 provides the variation of the factor N_σ with m_i for different values of *GSI* for a circular footing for 2 different values of q/σ_c, namely, 0.25 and 1. Similar to $N_{\sigma 0}$, the factor N_σ increases with an increase in the values of *GSI* and m_i. For a rough footing, the factor N_σ becomes greater than the corresponding values for a smooth footing. Figure 3 also provides a comparison between the present results and that computed by Chakraborty and Kumar.[7] It can be seen that for values of $GSI \geq 50$, the results from the present study become very close to the solution given by Chakraborty and Kumar.[7] For different values of *GSI*, $\sigma_c/(2\gamma b)$, and m_i, a comparison between the present values of N_σ and that given by Clausen[6] for a rough circular footing is presented in Table 2. The present results become very close to that given by Clausen.[6] The maximum difference between the 2 solutions has been found to be 2.2%.

For a strip footing, the bearing capacity factor $N_{\sigma 0}$ for a weightless rock mass has been presented in Table 3 for different values of *GSI* and m_i. For a strip footing, the roughness of the footing hardly affects the values of $N_{\sigma 0}$. This table also shows a comparison between the present values for $N_{\sigma 0}$ and those reported by (1) Merifield et al[4] and (2)

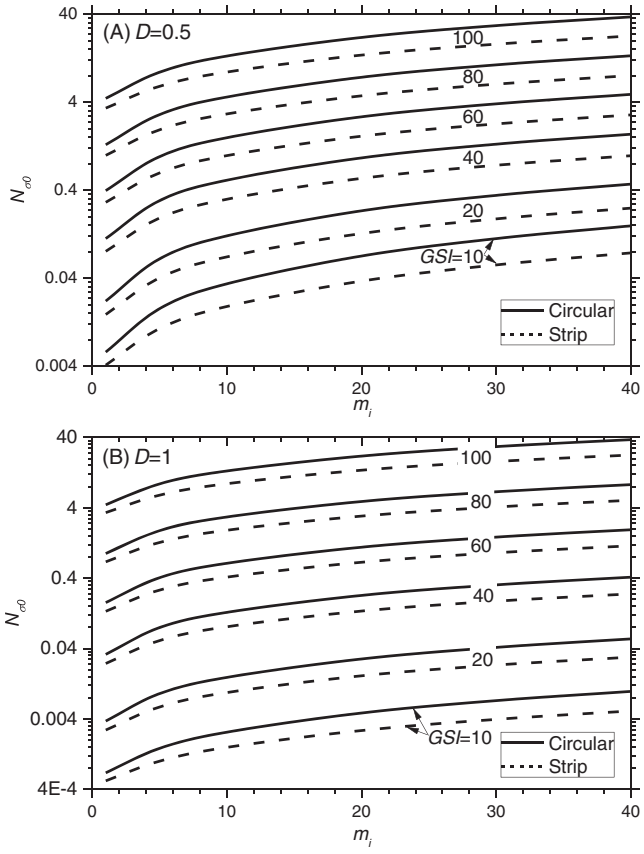

FIGURE 6 The variation of $N_{\sigma 0}$ with m_i and *GSI* for rough circular and strip footings for (A) $D = 0.5$ and (B) $D = 1$

Chakraborty and Kumar.[7] Note that the present results remain very close to the solutions of Merifield et al[4] and Chakraborty and Kumar.[7]

To evaluate the effect of the rock mass unit weight on the ultimate bearing capacity, Figures 4 and 5 have been drawn for the variation of $N_\sigma/N_{\sigma 0}$ with m_i corresponding to different values of $\sigma_c/(\gamma b)$ with 2 different magnitudes of *GSI*, namely, 10 and 50. Note that the ratio $N_\sigma/N_{\sigma 0}$ decreases continuously with an increase in the value of $\sigma_c/(\gamma b)$. For a weightless rock mass, $\sigma_c/(\gamma b) = \infty$, the magnitude of N_σ becomes simply equal to $N_{\sigma 0}$. The factor $N_\sigma/N_{\sigma 0}$ for a strip footing is found to be greater than that for a circular footing corresponding to the same values of $\sigma_c/(\gamma b)$, *GSI*, m_i, and q/σ_c. Furthermore, the rock mass unit weight has been found to have more effect for smaller values of $\sigma_c/(\gamma b)$, *GSI*, m_i, and q/σ_c.

Figure 6 presents the influence of the disturbance factor D on the factor $N_{\sigma 0}$ for rough circular and strip footings. It can be seen that the factor $N_{\sigma 0}$ decreases with an increase in the value of D.

6.3 | Pressure distribution below the footing base

For $\sigma_c/(\gamma b) = 250$, Figure 7A,B illustrates the normalized pressure distribution (q/σ_c) below the footing base for different values of m_i corresponding to circular and strip footing, respectively. Note that as compared with a smooth footing, the magnitude of the pressure becomes greater for a rough footing. It can be seen that the pressure distribution below the footing base does not become either uniform or linear. The maximum value of q_f, in all the cases, has been found to occur at the center of the circular footing. Around the center of the footing, the shape of the pressure distribution tends to become concave and convex, corresponding to circular and strip footings, respectively. Note that as compared with a strip footing, the magnitude of the normalized pressure becomes greater for a circular footing. Figure 8 also shows the pressure distribution below the footing base for smooth and rough strip and circular footings but for different values of $\sigma_c/(\gamma b)$. It can be seen that the magnitude of the pressure decreases continuously with an increase in the value of $\sigma_c/(\gamma b)$. Note that for the strip footing, the difference between the values of pressure of the smooth and rough footings

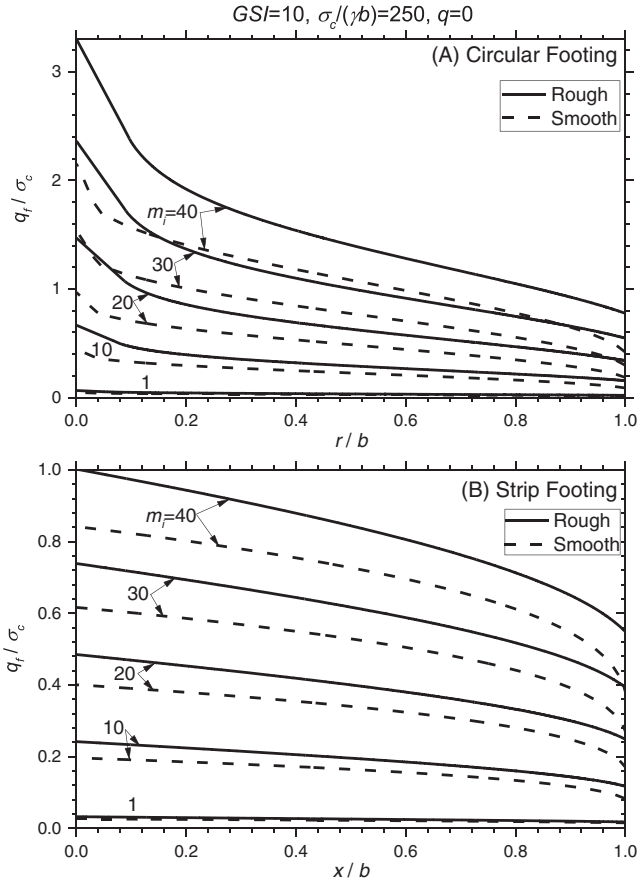

FIGURE 7 The pressure distribution below the footing base for different values of m_i with *GSI* = 10 and $\sigma_c/(\gamma b) = 250$ for (A) circular footing and (B) strip footing

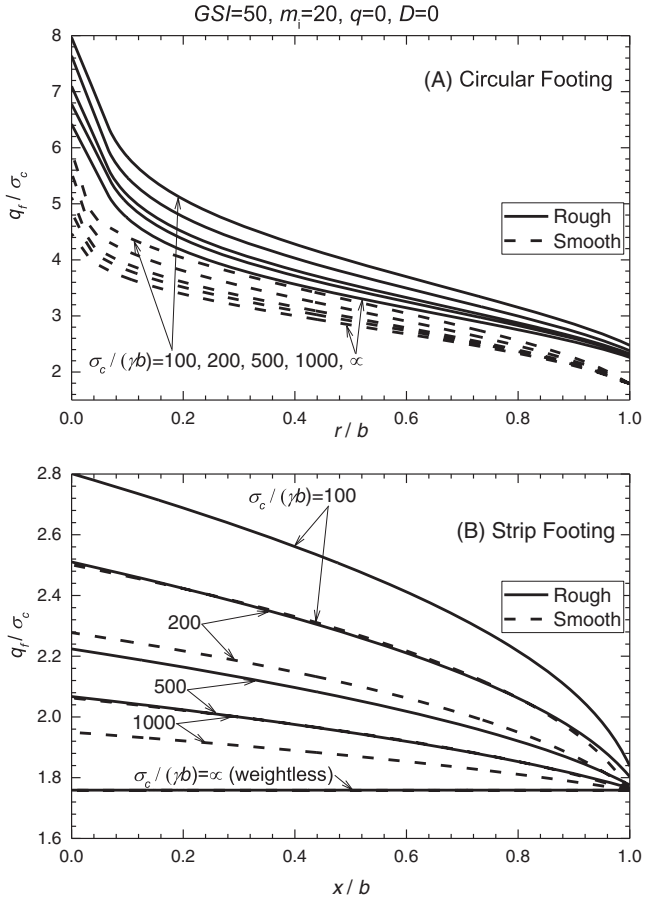

FIGURE 8 The pressure distribution below the footing base for different values of $\sigma_c/(\gamma b)$ with $GSI = 50$ and $m_i = 20$ for (A) circular footing and (B) strip footing

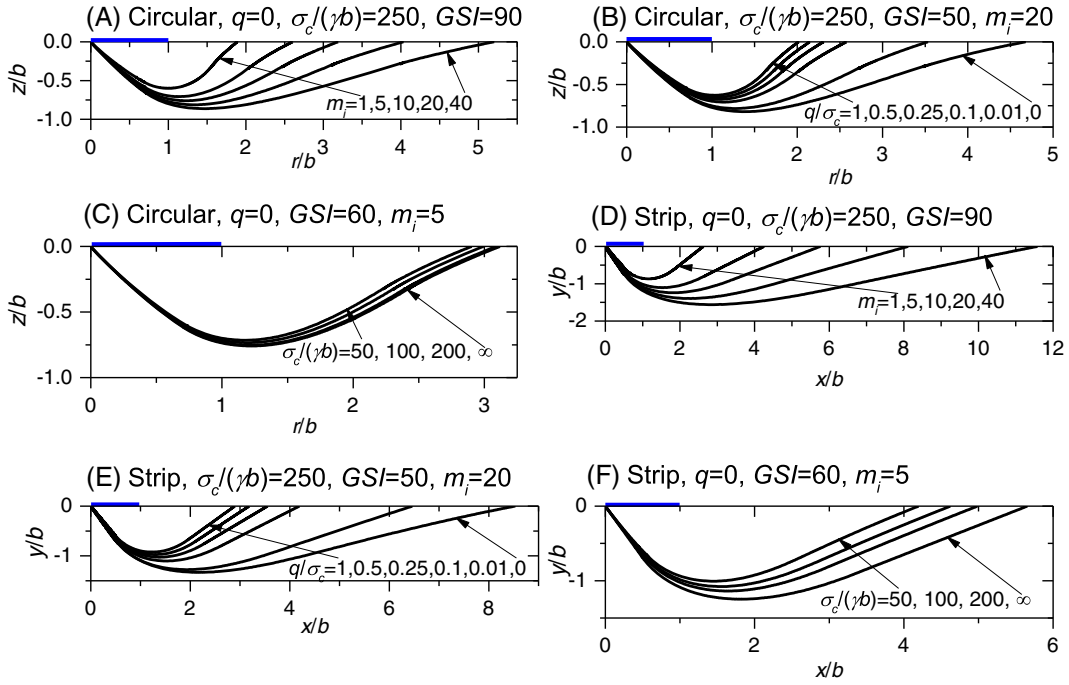

FIGURE 9 The effect of m_i, q/σ_c, and $\sigma_c/(\gamma b)$ on the failure patterns for circular and strip footings with smooth base [Colour figure can be viewed at wileyonlinelibrary.com]

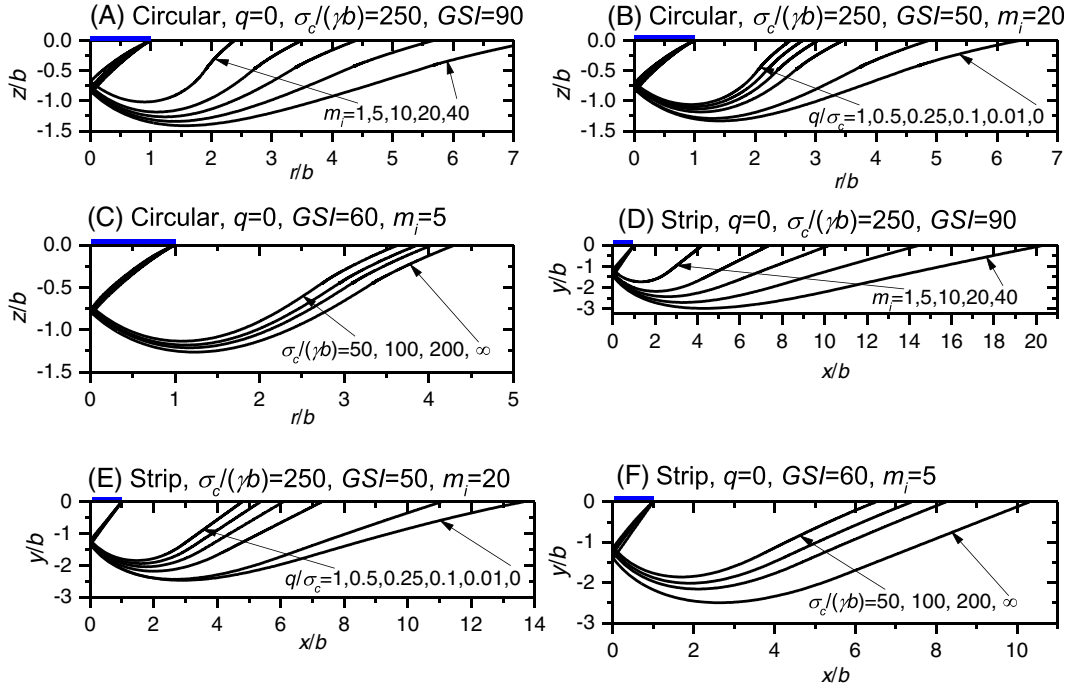

FIGURE 10 The effects of m_i, q/σ_c, and $\sigma_c/(\gamma b)$ on the failure patterns for circular and strip footings with rough base [Colour figure can be viewed at wileyonlinelibrary.com]

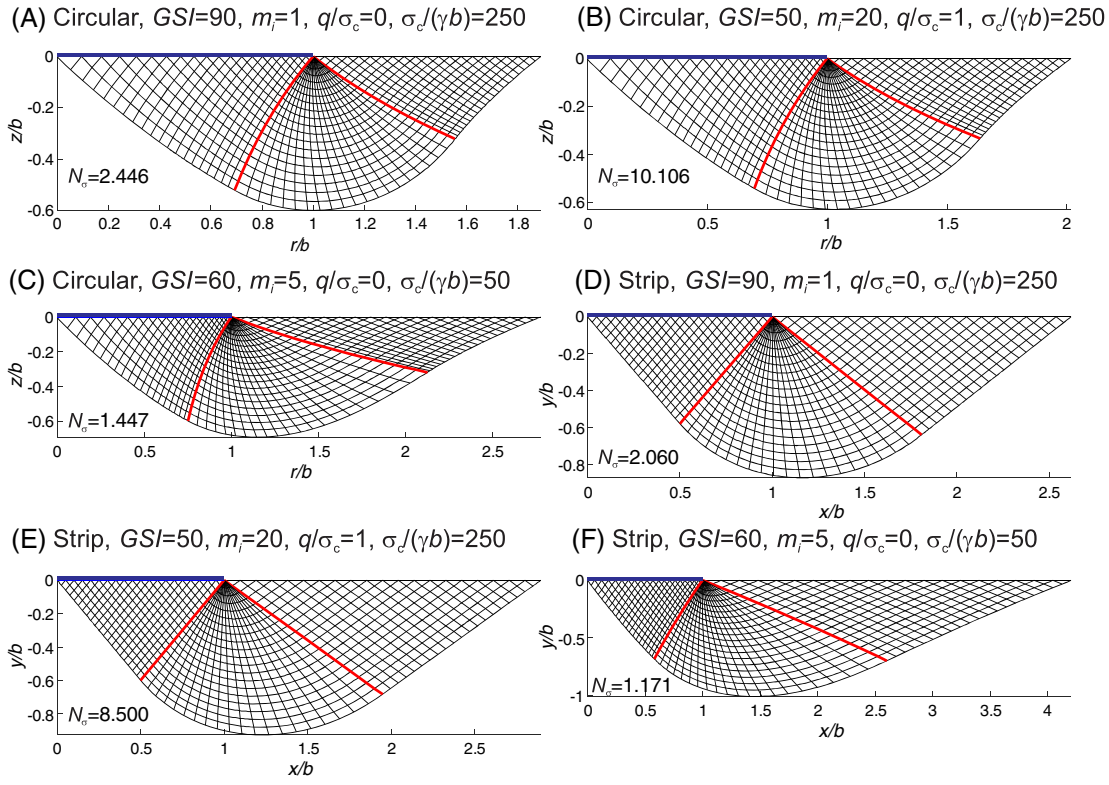

FIGURE 11 Complete slip patterns for circular and strip footings with smooth base [Colour figure can be viewed at wileyonlinelibrary.com]

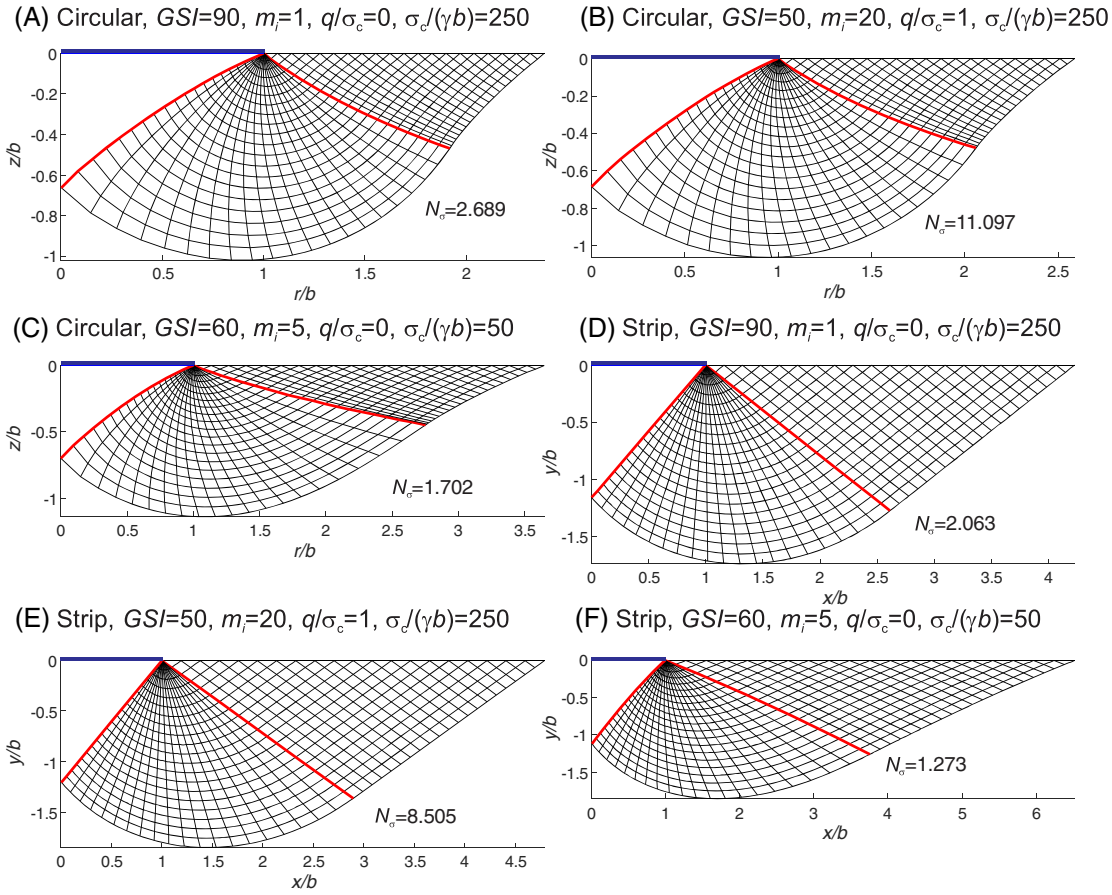

FIGURE 12 Complete slip patterns for circular and strip footings with rough base [Colour figure can be viewed at wileyonlinelibrary.com]

decreases with an increase in $\sigma_c/(\gamma b)$ and for the weightless rock mass, the pressure distributions of the smooth and rough strip footings are almost the same.

6.4 | Failure patterns

One of the significant advantages of the method of stress characteristics is that the failure patterns are automatically generated as a part of the solution during the process of computing the state of stress everywhere within the plastic domain. The effects of the different input parameters, namely, $\sigma_c/(\gamma b)$, m_i, and q/σ_c, on the slip line patterns are shown in Figures 9 and 10 for smooth and rough footings, respectively; the parts A to C present the slip line patterns for a circular footing, and the parts D to F show the corresponding patterns for a strip footing. These two figures are also redrawn in Figures 11 and 12 to provide the complete fan of slip patterns for a few typical cases. The selected input parameters for each case are indicated in these figures. It can be observed that with an increase in m_i, the size of the plastic zone extends continuously, and accordingly, the extent of the failure surface at the ground surface also increases. The effect of $\sigma_c/(\gamma b)$ on the slip line patterns was noted to be similar to that of m_i. However, the parameter q/σ_c was found to have a reverse effect on the slip line patterns (Figure 9B,E). For the same parameters, the extent of the failure surface for a rough footing is found to be greater than that for a smooth footing. In terms of normalized axes, a strip footing provides more extension of the slip line patterns as compared with the corresponding circular footing with the same input parameters.

7 | CONCLUSIONS

The ultimate bearing capacity of circular and strip footings, placed over rock mass, has been numerically evaluated by using the method of stress characteristics for both smooth and rough footing-rock interface. The modified HB failure

criterion, which is the widely accepted yield basis to characterize the rock mass, was used in the analysis. Various steps have been provided in detail for describing the procedure. The bearing capacity has been presented in the form of non-dimensional bearing capacity factors as a function of different input parameters for rock mass. It has been clearly noted that an increase of *GSI* and m_i leads to an increase in the values of N_σ and $N_{\sigma 0}$. An increase in the surcharge pressure causes a further increase in the values of both N_σ and $N_{\sigma 0}$. The factor N_σ has been found to increase continuously with a decrease in the value of $\sigma_c/(\gamma b)$. The roughness of the footing has been found to have more significant effect for a circular footing as compared with a strip footing. The results obtained from the present study have been found to compare quite well with the different solutions available from literature.

ORCID

Amin Keshavarz http://orcid.org/0000-0002-8951-9233
Jyant Kumar http://orcid.org/0000-0002-7808-8984

REFERENCES

1. Serrano A, Olalla C. Ultimate bearing capacity of rock masses. *Int J Rock Mech Min Sci*. 1994;31(2):93-106. https://doi.org/10.1016/0148-9062(94)92799-5
2. Serrano A, Olalla C, Gonzalez J. Ultimate bearing capacity of rock masses based on the modified Hoek-Brown criterion. *Int J Rock Mech Min Sci*. 2000;37(6):1013-1018. https://doi.org/10.1016/S1365-1609(00)00028-9
3. Yang X, Yin JH, Li L. Influence of a nonlinear failure criterion on the bearing capacity of a strip footing resting on rock mass using a lower bound approach. *Canadian Geotechnical Journal*. 2003;40(3):702-707. https://doi.org/10.1139/t03-010
4. Merifield R, Lyamin A, Sloan S. Limit analysis solutions for the bearing capacity of rock masses using the generalised Hoek-Brown criterion. *Int J Rock Mech Min Sci*. 2006;43(6):920-937. https://doi.org/10.1016/j.ijrmms.2006.02.001
5. Zhou XP, Yang HQ, Zhang YX, Yu MH. The effect of the intermediate principal stress on the ultimate bearing capacity of a foundation on rock masses. *Computers and Geotechnics*. 2009;36(5):861-870. https://doi.org/10.1016/j.compgeo.2009.01.009
6. Clausen J. Bearing capacity of circular footings on a Hoek-Brown material. *Int J Rock Mech Min Sci*. 2013;57:34-41. https://doi.org/10.1016/j.ijrmms.2012.08.004
7. Chakraborty M, Kumar J. Bearing capacity of circular footings over rock mass by using axisymmetric quasi lower bound finite element limit analysis. *Computers and Geotechnics*. 2015;70:138-149. https://doi.org/10.1016/j.compgeo.2015.07.015
8. Keshavarz A, Fazeli A, Sadeghi S. Seismic bearing capacity of strip footings on rock masses using the Hoek-Brown failure criterion. *J Rock Mech Geotech Eng*. 2016;8(2):170-177. https://doi.org/10.1016/j.jrmge.2015.10.003
9. Hoek E, Wood D, Shah S. A modified Hoek-Brown criterion for jointed rock masses. in Proc. Rock Characterization, Symp. Int. Soc. Rock Mech.: Eurock. 1992.
10. Hoek E, Carranza-Torres C, Corkum B. Hoek-Brown failure criterion-2002 edition. in Proceedings of NARMS-Tac. 2002.
11. Booker J, Davis E. A general treatment of plastic anisotropy under conditions of plane strain. *J Mech Phys Solids*. 1972;20(4):239-250. https://doi.org/10.1016/0022-5096(72)90003-8
12. Jahanandish M, Keshavarz A. Seismic bearing capacity of foundations on reinforced soil slopes. *Geotextiles and Geomembranes*. 2005;23(1):1-25. https://doi.org/10.1016/j.geotexmem.2004.09.001
13. Kumar J. $N\gamma$ for rough strip footing using the method of characteristics. *Canadian Geotechnical Journal*. 2003;40(3):669-674. https://doi.org/10.1139/t03-009
14. Lundgren H, Mortensen K. Determination by the theory of plasticity of the bearing capacity of continuous footings on sand. in Proceedings of the Third International Conference on Soil Mechanics and Foundation Engineering. 1953. Zürich, Switzerland.
15. Martin CM. Exact bearing capacity calculations using the method of characteristics. Proc. IACMAG. Turin 2005:441–450.
16. Clausen J. Discussion on "bearing capacity of circular footings over rock mass by using axisymmetric quasi lower bound finite element limit analysis" by Chakraborty M and Kumar J. *Computers and Geotechnics*. 2016;73:231-234. https://doi.org/10.1016/j.compgeo.2015.12.002

How to cite this article: Keshavarz A, Kumar J. Bearing capacity of foundations on rock mass using the method of characteristics. *Int J Numer Anal Methods Geomech*. 2018;42:542-557. https://doi.org/10.1002/nag.2754